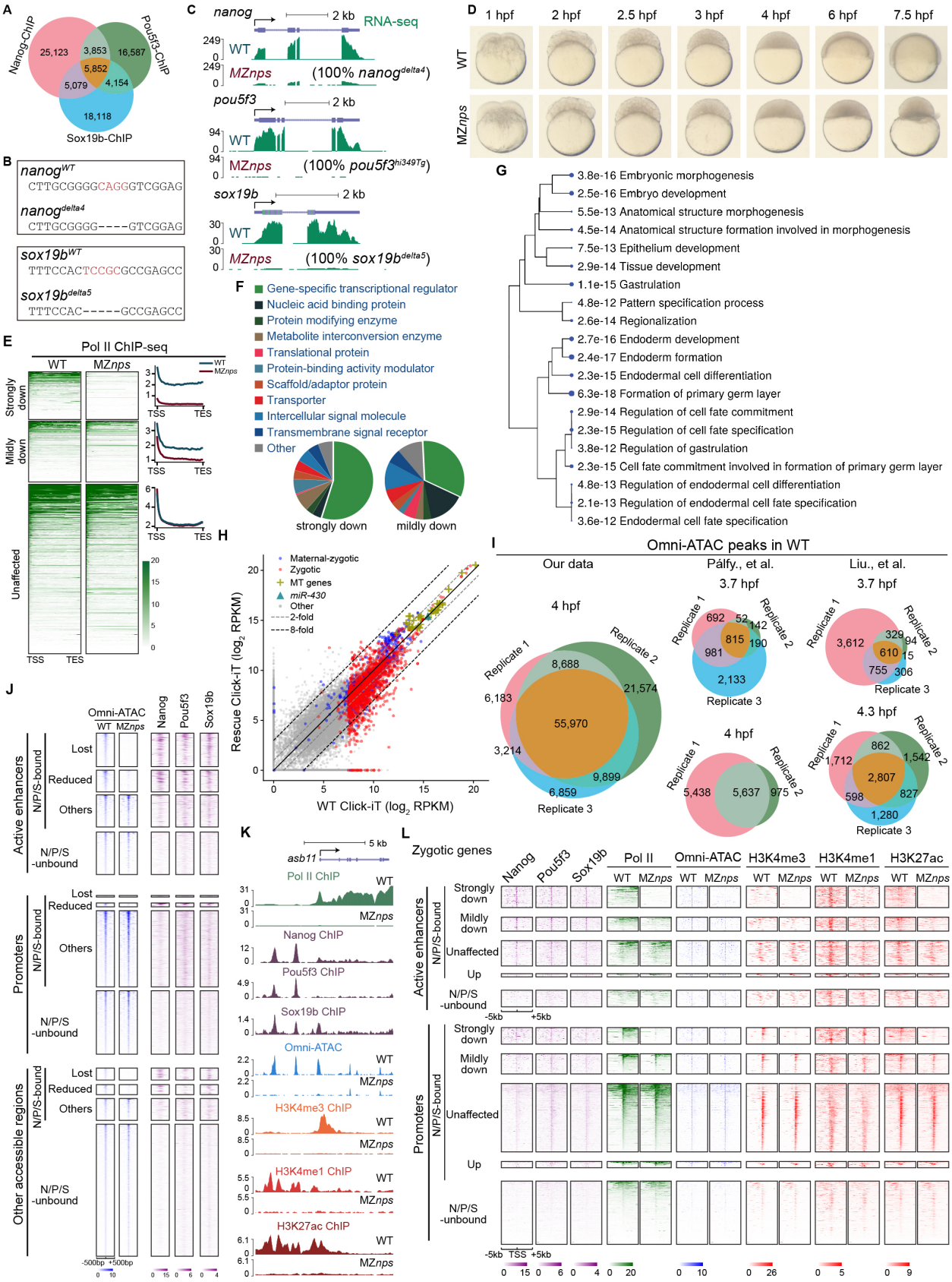
A
Nanog-ChIP
Pou5f3-ChIP
Sox19b-ChIP
25,123
3,853
16,587
5,852
5,079
4,154
18,118
B
nanog^WT
CTTGCGGGGCAGGGTCGGAG
nanog^delta4
CTTGCGGGG----GTCGGAG
sox19b^WT
TTTCCACTCCGCGCCGAGCC
sox19b^delta5
TTTCCAC-----GCCGAGCC
C
nanog
2 kb
RNA-seq
WT
MZnps
(100% nanog^delta4)
pou5f3
(100% pou5f3^hi349Tg)
sox19b
(100% sox19b^delta5)
D
1 hpf
2 hpf
2.5 hpf
3 hpf
4 hpf
6 hpf
7.5 hpf
WT
MZnps
E
Pol II ChIP-seq
WT
MZnps
Strongly down
Mildly down
Unaffected
TSS
TES
F
Gene-specific transcriptional regulator
Nucleic acid binding protein
Protein modifying enzyme
Metabolite interconversion enzyme
Translational protein
Protein-binding activity modulator
Scaffold/adaptor protein
Transporter
Intercellular signal molecule
Transmembrane signal receptor
Other
strongly down
mildly down
G
3.8e-16 Embryonic morphogenesis
2.5e-16 Embryo development
5.5e-13 Anatomical structure morphogenesis
4.5e-14 Anatomical structure formation involved in morphogenesis
7.5e-13 Epithelium development
2.9e-14 Tissue development
1.1e-15 Gastrulation
4.8e-12 Pattern specification process
2.6e-14 Regionalization
2.7e-16 Endoderm development
2.4e-17 Endoderm formation
2.3e-15 Endodermal cell differentiation
6.3e-18 Formation of primary germ layer
2.9e-14 Regulation of cell fate commitment
2.3e-15 Regulation of cell fate specification
3.8e-12 Regulation of gastrulation
2.3e-15 Cell fate commitment involved in formation of primary germ layer
4.8e-13 Regulation of endodermal cell differentiation
2.1e-13 Regulation of endodermal cell fate specification
3.6e-12 Endodermal cell fate specification
H
Maternal-zygotic
Zygotic
MT genes
miR-430
Other
2-fold
8-fold
Rescue Click-iT (log2 RPKM)
WT Click-iT (log2 RPKM)
I
Omni-ATAC peaks in WT
Our data
Pálfy., et al.
Liu., et al.
4 hpf
3.7 hpf
4.3 hpf
Replicate 1
Replicate 2
Replicate 3
8,688
21,574
6,183
55,970
3,214
9,899
6,859
692
52
142
815
190
981
2,133
3,612
329
94
610
15
755
306
5,438
5,637
975
862
1,542
1,712
2,807
598
827
1,280
J
Omni-ATAC
WT
MZnps
Nanog
Pou5f3
Sox19b
Active enhancers
Promoters
Other accessible regions
N/P/S-bound
N/P/S -unbound
Lost
Reduced
Others
-500bp
+500bp
K
asb11
5 kb
Pol II ChIP
Nanog ChIP
Pou5f3 ChIP
Sox19b ChIP
Omni-ATAC
H3K4me3 ChIP
H3K4me1 ChIP
H3K27ac ChIP
L
Zygotic genes
Nanog
Pou5f3
Sox19b
Pol II
Omni-ATAC
H3K4me3
H3K4me1
H3K27ac
Strongly down
Mildly down
Unaffected
Up
N/P/S -unbound
-5kb
TSS
+5kb

Figure S1. Nanog, Pou5f3, and Sox19b are required for chromatin remodeling and histone modification during genome activation, Related to Figure 1.

(A) Venn diagrams showing significant overlap of NPS binding, as assayed by ChIP-seq at 4 hpf (Fisher's exact test, $P < 1\times10^{-100}$).

(B) DNA sequences of wild-type (WT) and mutant alleles for *nanog* mutant (*nanog*^{delta4}) and *sox19b* mutant (*sox19b*^{delta5}), generated with the CRISPR/Cas9 system.

(C) Genomic tracks of RNA-seq showing *nanog*, *pou5f3*, and *sox19b* expression in WT and MZ*nps* embryos. All the reads from MZ*nps* embryos that are mapped to *nanog*, *pou5f3*, and *sox19b* are mutant allele (*nanog*^{delta4}, *pou5f3*^{hi349Tg}, *sox19b*^{delta5}).

(D) A time course of the developmental phenotypes of WT and MZ*nps* embryos at 1 hpf, 2 hpf, 2.5 hpf, 3 hpf, 4 hpf, 6 hpf, and 7.5 hpf.

(E) Heatmaps and line plots showing Pol II binding along the gene body of differentially affected zygotic genes in wild-type (WT) and MZ*nps* embryos. Each zygotic gene was grouped into 100 bins from the TSS to the TES (transcription end site, annotated from Ensembl) and Pol II signal was averaged within each bin. See Figure 1C for explanation of different categories.

(F) Protein class enrichment of the strongly and mildly downregulated genes as determined by PANTHER gene ontology enrichment analysis.

(G) Hierarchical clustering tree showing the correlation among the top 20 significantly enriched biological processes for the strongly downregulated genes. Analysis was performed using ShinyGO gene ontology enrichment analysis. Biological processes are clustered together based on shared genes. Dot size indicates *P*-value: a larger size represents a lower *P*-value.

(H) Biplot comparing the nascent transcriptome of MZ*nps* embryos rescued with *nanog* and *pou5f3* mRNAs (Rescue) with that of WT embryos.

(I) Venn diagrams showing high reproducibility across three replicates of Omni-ATAC in WT embryos at 4 hpf and the overlap of previously published ATAC-seq peaks between replicates in WT embryos at 3.7 and 4.3 hpf.

(J) Heatmaps showing NPS binding and accessibility (Omni-ATAC) in WT and MZ*nps* embryos at accessible chromatin regions. Lost: chromatin accessibility lost in MZ*nps* embryos; Reduced: chromatin accessibility reduced; Others: accessible regions that are unaffected or upregulated in MZ*nps* embryos. Heatmaps are centered at the summit of Omni-ATAC peaks with 500bp on both sides and are ranked according to the average intensity of the Omni-ATAC signal in WT.

(K) Representative genome tracks of Pol II binding, Omni-ATAC, and H3K4me1, H3K4me3, and H3K27ac levels in WT and MZ*nps* embryos, along with NPS binding in WT embryos around the *asb11* locus.

(L) Heatmaps showing NPS and Pol II ChIP-seq signal, accessibility (Omni-ATAC), and H3K4me1, H3K4me3, and H3K27ac levels at active enhancer and promoter regions of differentially affected zygotic genes in WT and MZ*nps* embryos. Heatmaps are centered at the TSS (for promoters) and the summit of the Omni-ATAC peak (for active enhancers) with the flanking 5kb on both sides and ranked according to the average intensity of Pol II binding within +/- 1kb from the TSS of the associated zygotic genes in WT embryos. Number of promoters and active enhancers in each category: Promoter (strongly down: 213; mildly down: 259; unaffected: 876; up: 82; N/P/S-unbound: 810); Active enhancer (strongly down: 274; mildly down: 179; unaffected: 324; up: 41; N/P/S-unbound: 215)

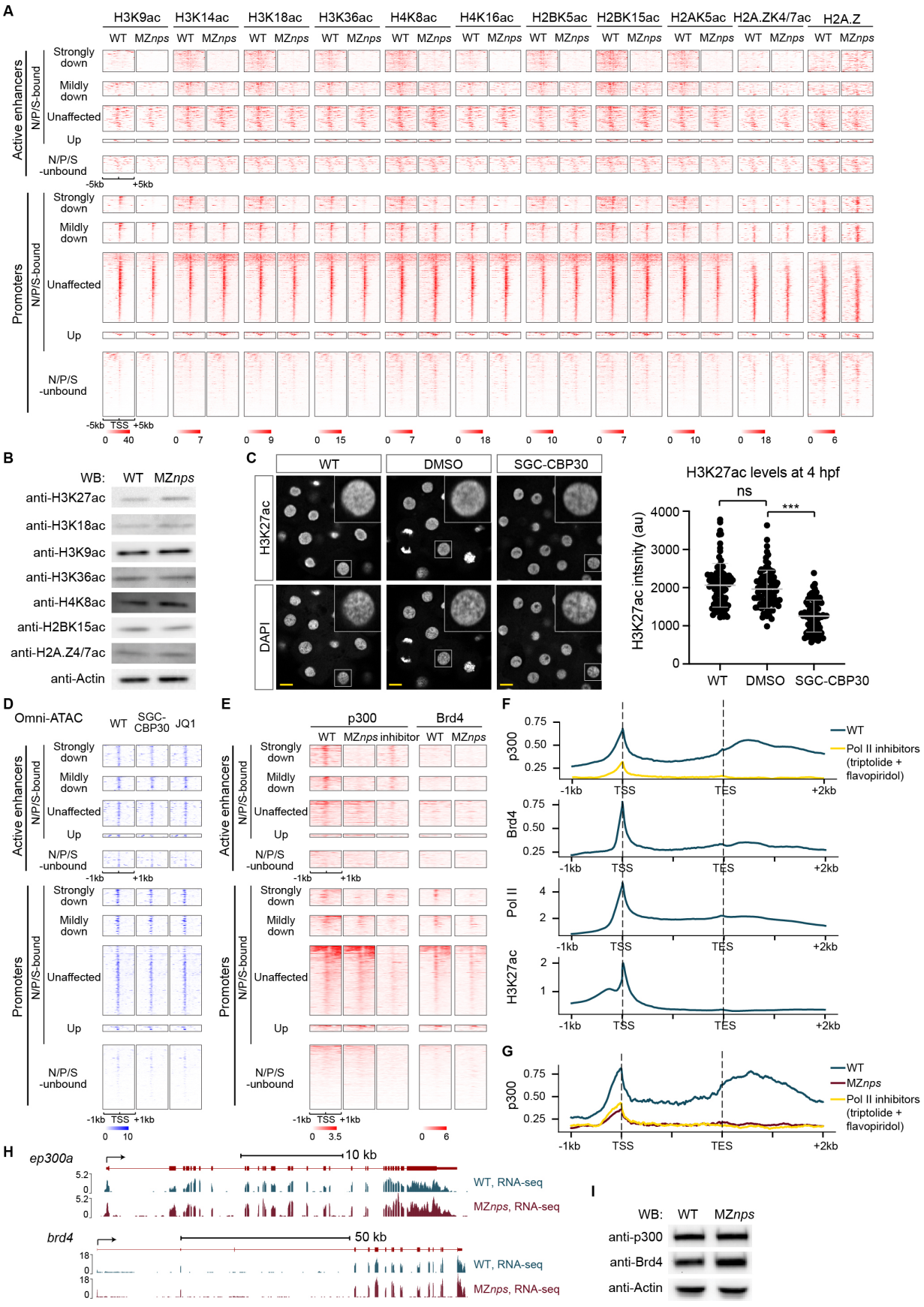
A
H3K9ac
H3K14ac
H3K18ac
H3K36ac
H4K8ac
H4K16ac
H2BK5ac
H2BK15ac
H2AK5ac
H2A.ZK4/7ac
H2A.Z
WT MZnps
Active enhancers
N/P/S-bound
Promoters
Strongly down
Mildly down
Unaffected
Up
N/P/S -unbound
-5kb +5kb
TSS
B
WB: WT MZnps
anti-H3K27ac
anti-H3K18ac
anti-H3K9ac
anti-H3K36ac
anti-H4K8ac
anti-H2BK15ac
anti-H2A.Z4/7ac
anti-Actin
C
WT
DMSO
SGC-CBP30
H3K27ac
DAPI
H3K27ac levels at 4 hpf
ns
***
H3K27ac intsnity (au)
D
Omni-ATAC
WT
SGC-CBP30
JQ1
E
p300
Brd4
MZnps inhibitor
F
p300
Brd4
Pol II
H3K27ac
-1kb
TSS
TES
+2kb
WT
Pol II inhibitors (triptolide + flavopiridol)
G
MZnps
H
ep300a
10 kb
WT, RNA-seq
MZnps, RNA-seq
brd4
50 kb
I
anti-p300
anti-Brd4

Figure S2. Nanog, Pou5f3, and Sox19b are required for histone acetylation across core histones and for recruitment of p300 and Brd4, Related to Figure 2.

(A) Heatmaps showing histone acetylation levels across canonical core histones and the histone H2A variant H2A.Z at active enhancers and promoters of differentially affected zygotic genes in wild-type (WT) and MZ*nps* embryos. Heatmaps are centered at the TSS (for promoters) and the summit of the Omni-ATAC peak (for active enhancers) with the flanking 5kb on both sides and ranked according to the average intensity of Pol II binding within +/- 1kb from the TSS of the associated zygotic genes in WT embryos. ChIP-seq analysis revealed that H2A.Z levels are significantly upregulated at NPS strong target genes in MZ*nps* mutants (Figure 2A; Wilcoxon sign-ranked test, $P < 10^{-12}$), while the levels of H2A.ZK4/7ac and the proportion of acetylated H2A.Z (H2A.ZK4/7ac / H2A.Z) are significantly reduced (Wilcoxon sign-ranked test, $P < 10^{-9}$ and $P < 10^{-28}$ respectively), suggesting that NPS regulates H2A.Z acetylation.

(B) Western blot showing the protein level of acetylated histones in WT and MZ*nps* embryos.

(C) Confocal imaging (left) and the quantification (right) of the H3K27ac immunofluorescence in SGC-CBP30 treated embryos. Images shown are single z slices. Scale bar: 10 μm. n ≥ 83 nuclei across three embryos (two-tailed unpaired t-test, ns: not significant, *** P <0.001).

(D) Heatmaps showing accessibility (Omni-ATAC) levels at active enhancer and promoter regions of differentially affected zygotic genes in SGC-CBP30 and JQ1 treated embryos. Heatmaps are centered at the TSS (for promoters) and the summit of the Omni-ATAC peak (for active enhancers) with the flanking 1kb on both sides and ranked according to the average intensity of Pol II binding within +/- 1kb from the TSS of the associated zygotic gene in WT embryos.

(E) Heatmaps showing p300 and Brd4 levels at active enhancers and promoters of differentially affected zygotic genes. Heatmaps are centered at the TSS (for promoters) and the summit of the Omni-ATAC peak (for active enhancers) with the flanking 1kb on both sides and ranked according to the average intensity of Pol II binding within +/- 1kb from the TSS of the associated zygotic gene in WT embryos. inhibitor: embryos treated with Pol II inhibitors (triptolide + flavopiridol).

(F-G) Line plots from 1kb upstream of the TSS to 2kb downstream of the TES showing p300, Brd4, Pol II, and H3K27ac binding at all zygotic genes (F) and p300 binding at NPS strong targets (G). Each zygotic gene body was grouped into 200 bins from the TSS to the TES and ChIP-seq signal was averaged within each bin. Zygotic genes with length < 200 bp were not included.

(H) Genomic tracks of RNA-seq showing *ep300a* and *brd4* expression in WT and MZ*nps* embryos.

(I) Western blot showing the protein level of p300 and Brd4 in WT and MZ*nps* embryos.

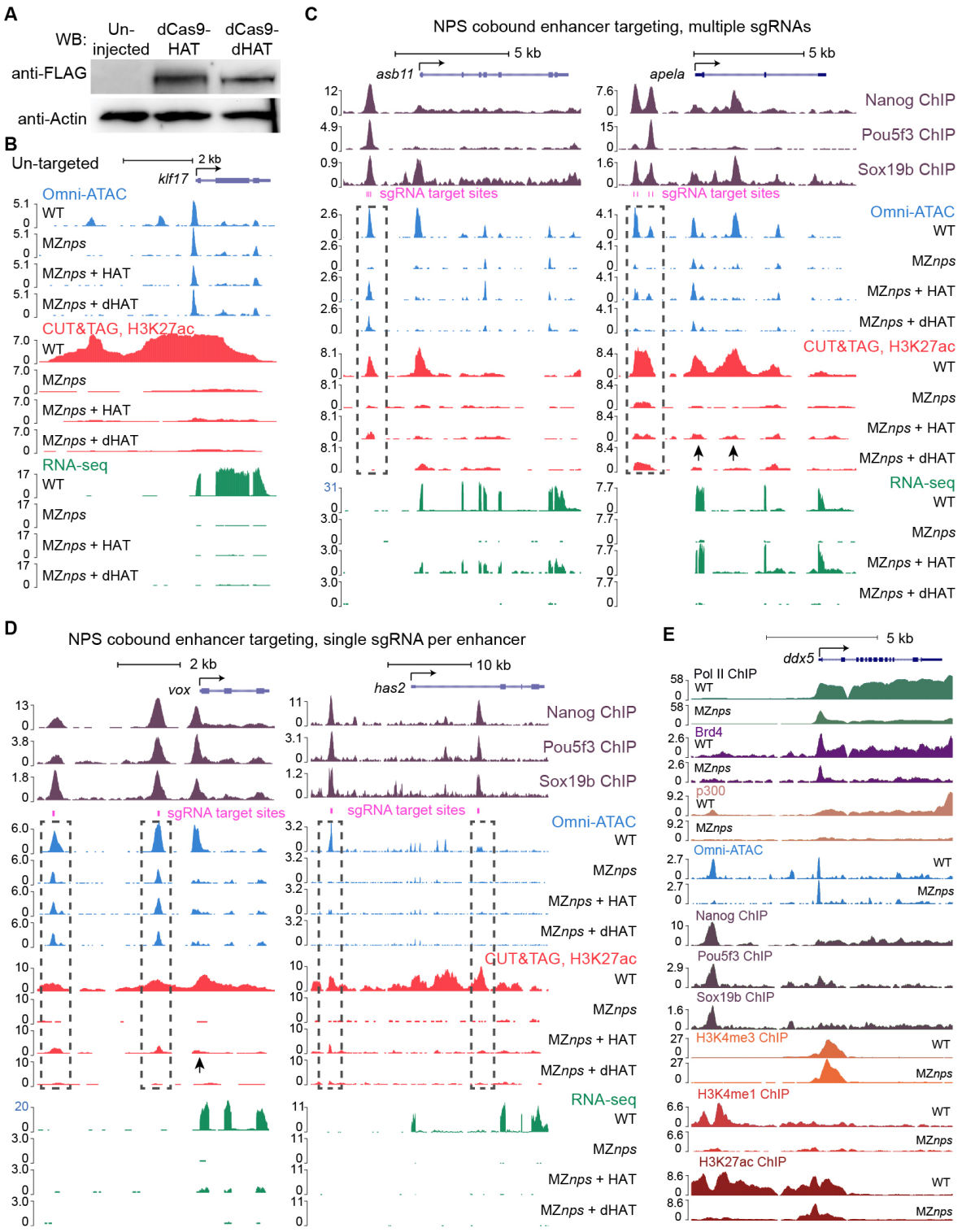

Figure S3. Restoration of histone acetyltransferase activity partially rescues transcription of NPS strong targets, Related to Figure 3.

(A) Western blot showing the expression of dCas9-HAT (3xFLAG-dCas9-p300 Core) and dCas9-dHAT (3xFLAG-dCas9-p300 Core, D1399Y) in zebrafish embryos.
(B) Genomic tracks of a control gene, *klf17*, which was not targeted by the dCas9-HAT system. H3K27ac and transcription levels were largely downregulated in MZ*nps* embryos compared with that in wild-type (WT) embryos. dCas9-HAT did not restore H3K27ac or transcription in the absence of *klf17*-specific sgRNAs.
(C-D) Genome tracks showing that accessibility, H3K27ac, and transcription were partially restored at different zygotic genes by specifically targeting the associated active enhancers using the dCas9-HAT system (C, multiple sgRNAs per enhancer; D, single sgRNA per enhancer). However, neither acetylation at the promoter nor transcriptional activation was restored at *has2*. The location of the sgRNAs used in each experiment is indicated in the track with magenta bars and the dashed line boxes. Arrows show regions where H3K27ac is rescued.
(E) Genome tracks of Pol II, Brd4 and P300 binding, NPS binding, accessibility (Omni-ATAC), H3K4me1, H3K4me3, and H3K27ac levels in WT and MZ*nps* embryos around the *ddx5* gene.

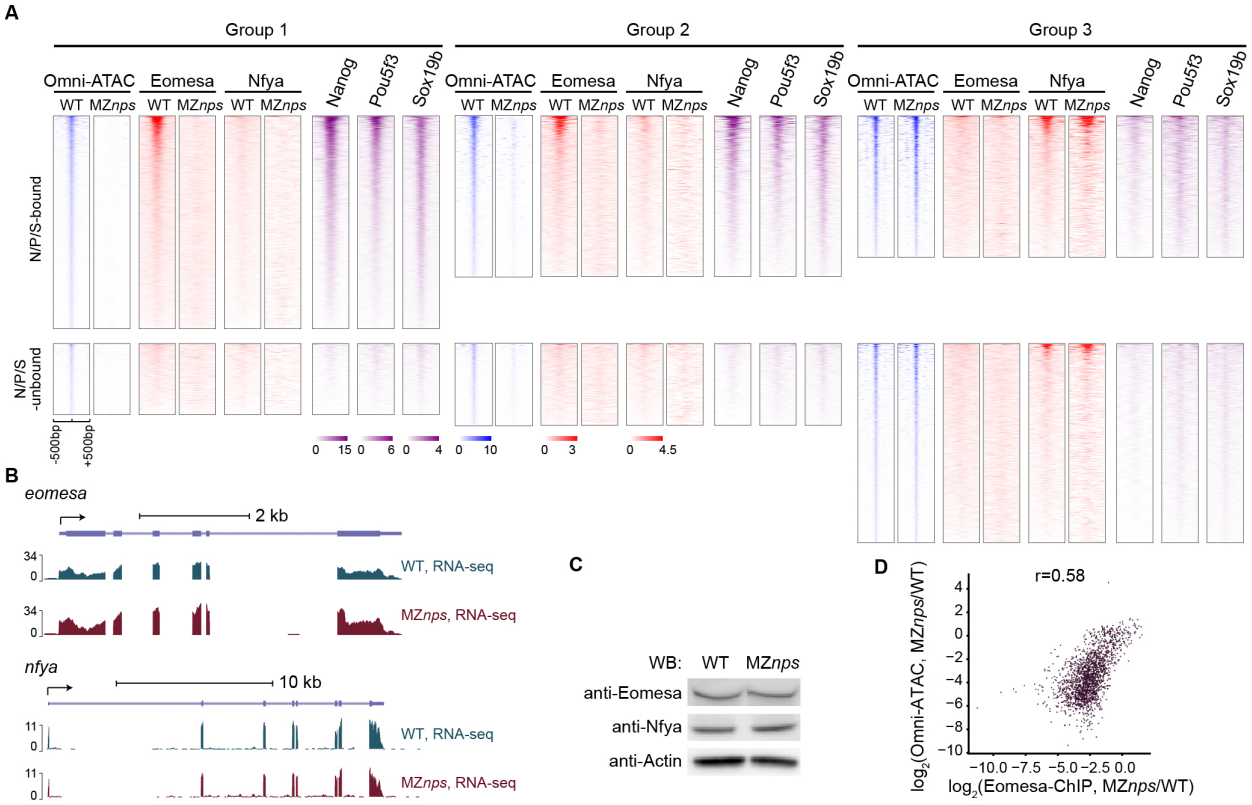

Figure S4. Eomesa and Nfya binding differentially depend on NPS pioneering function, Related to Figure 4.

(A) Heatmaps of Eomesa, Nfya, and NPS ChIP-seq signal and Omni-ATAC signal at differentially affected accessible regions (in Figure 4A) in wild-type (WT) and MZ*nps* embryos at N/P/S-bound and N/P/S-unbound regions. Heatmaps are centered at the summit of Omni-ATAC peaks with the flanking 500bp on both sides and are ranked according to the average intensity of ChIP-seq signal in WT embryos.

(B) Genomic tracks of RNA-seq showing *eomesa* and *nfya* expression in WT and MZ*nps* embryos.

(C) Western blot showing the protein level of Eomesa and Nfya in WT and MZ*nps* embryos.

(D) Biplot showing a high correlation between the reduction in Eomesa binding and accessibility loss in MZ*nps* embryos compared to that in WT embryos (r = 0.58, Pearson correlation).

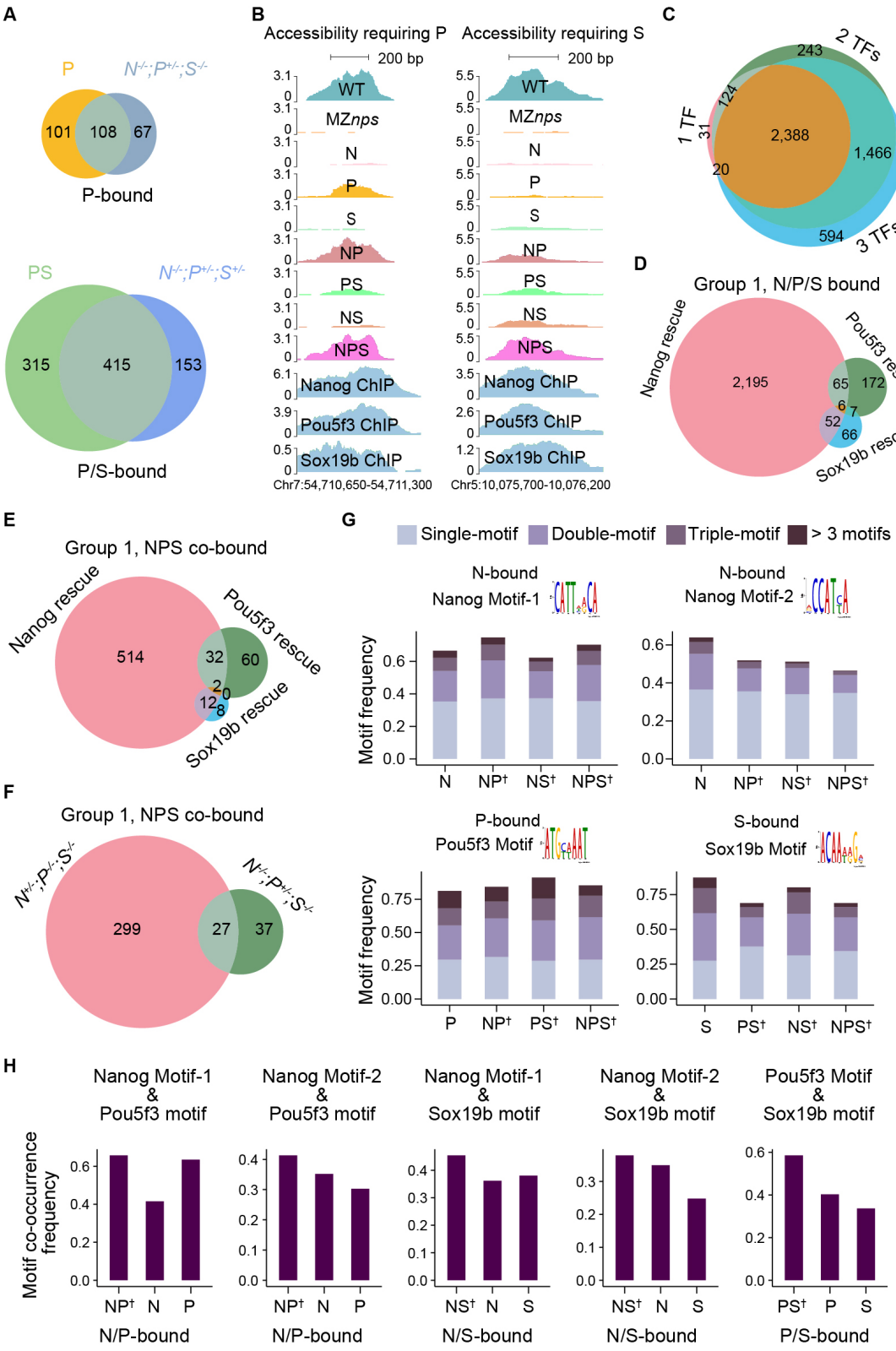

Figure S5. NPS function independently and cooperatively to remodel chromatin, Related to Figure 5.

(A) Venn diagrams showing significant overlap of Group 1 regions that can be rescued in different rescue conditions (indicated in the top left of each diagram) and corresponding genotypes (indicated in the top right of each diagram). (P ($P = 1.4 \times 10^{-86}$); PS ($P < 10^{-100}$); Fisher's exact test).

(B) Representative genome tracks showing accessibility in different rescue conditions at NPS co-bound regions that require P and S to rescue accessibility.

(C) Venn diagram showing the overlap of N/P/S-bound Group 1 regions that require one, two, or three NPS factors to rescue accessibility.

(D) Venn diagram showing the overlap of N/P/S-bound Group 1 regions that can be rescued with a single NPS factor.

(E) Venn diagram showing the overlap of Group 1 regions bound by all three factors (co-bound) that can be rescued with a single NPS factor.

(F) Venn diagram showing the overlap of Group 1 regions bound by all three factors (co-bound) that can be rescued in *nanog*$^{+/-}$;*pou5f3*$^{-/-}$;*sox19b*$^{-/-}$ and *nanog*$^{-/-}$;*pou5f*$^{+/-}$;*sox19b*$^{-/-}$ mutants.

(G) Stacked bar plots comparing the motif frequency between regions that can be rescued by a single factor, two factors only, or three factors only at Group 1 regions. †denotes that the combination of factors listed are required for rescue. Due to the high co-occupancy of Nanog and Pou5f3 and the similarity between their binding motifs, we identified a second Nanog motif (Nanog motif-2) from regions bound exclusively by Nanog and not by Pou5f3 and Sox19b (See Methods).

(H) Bar plots comparing motif co-occurrence between regions that can be rescued by a single factor and those that require two factors at Group 1 regions. Regions that require two factors have a higher frequency of motif co-occurrence for each factor compared to regions that can be rescued by a single factor.

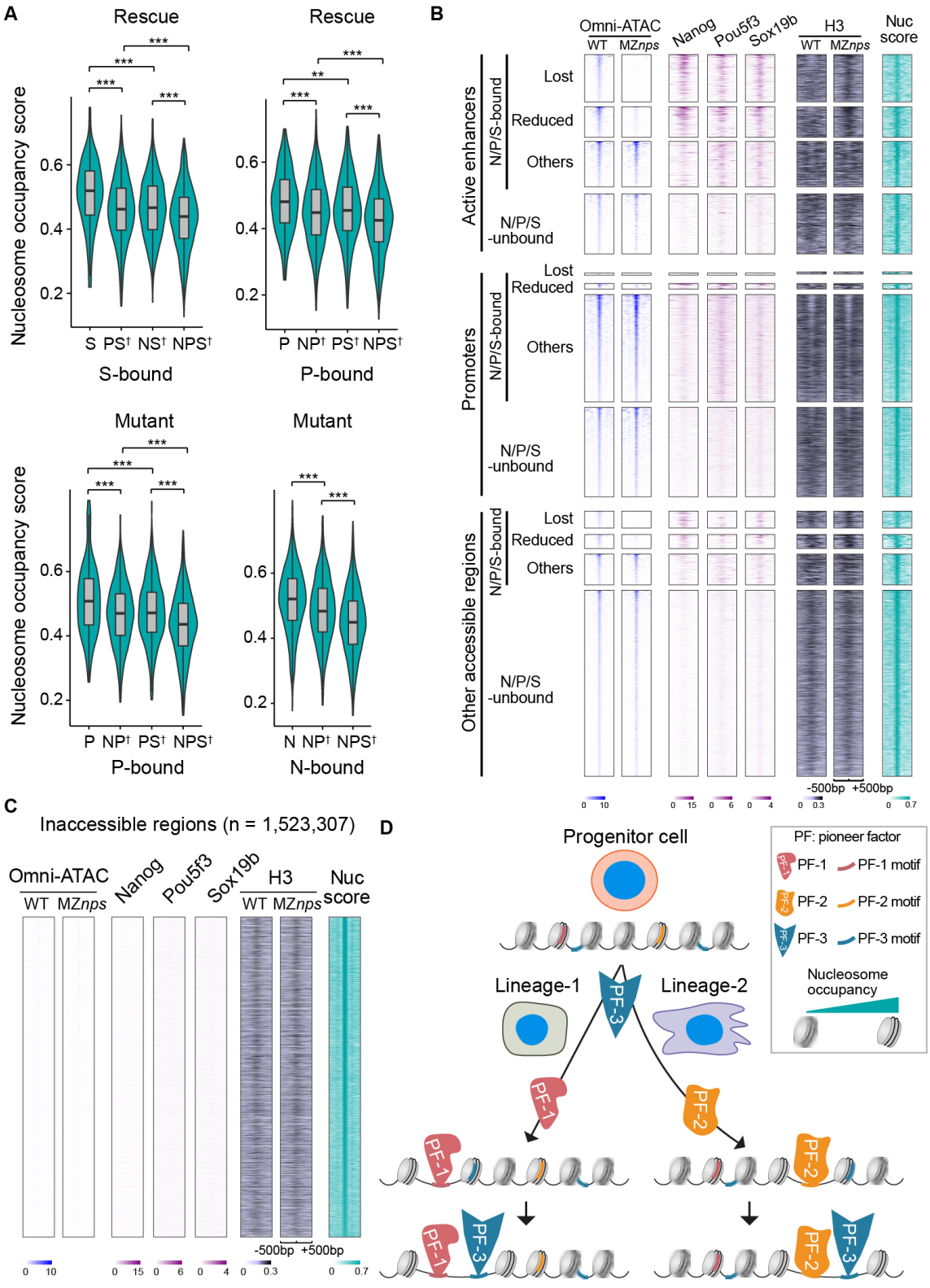

Figure S6. Nucleosome occupancy facilitates pioneering activity of Nanog, Pou5f3, and Sox19b, Related to Figure 6.

(A) Violin plots comparing the nucleosome occupancy scores between regions that can be rescued by a single, double, or triple factor combination and in corresponding genotypes at Group 1 regions. Regions that require multiple factors to be accessible have significantly lower nucleosome occupancy than regions that can be rescued by a single factor (two-sample t-test, ** P <0.01, *** P <0.001). On the x-axis, † denotes regions that require two or all three factors for rescue.
(B-C) Heatmaps showing NPS binding, accessibility (Omni-ATAC), nucleosome occupancy score and H3 ChIP signal in WT and MZ*nps* embryos at accessible regions (B) and nucleosome occupancy peaks (see Methods) that are inaccessible (C). Lost: chromatin accessibility lost in MZ*nps* embryos; Reduced: chromatin accessibility reduced; Others: accessible regions that are unaffected or upregulated in MZ*nps* embryos. Heatmaps are centered at the summit of Omni-ATAC peaks (B) and nucleosome occupancy peaks (C) with 500bp on both sides and are ranked according to the average intensity of the Omni-ATAC signal in WT (B) and nucleosome occupancy score (C).
(D) Schematic of a hypothesized model illustrating nucleosome remodeling by a cascade of pioneer factors across different cell lineages during development. The flexibility of nucleosome position provides a flexible platform for different pioneer factors to interpret the genome.